ORIGINAL ARTICLE

Investigating obesity-associated brain inflammation using quantitative water content mapping

Stephanie Kullmann[1,2,3] (ID) | Zaheer Abbas[4,5] | Jürgen Machann[1,2,6] | Nadim J. Shah[4,5,7,8,9] | Klaus Scheffler[10,11] | Andreas L. Birkenfeld[1,2,3] | Hans-Ulrich Häring[1,2,3] | Andreas Fritsche[1,2,3] | Martin Heni[1,2,3,12] | Hubert Preissl[1,2,3,13,14] (ID)

[1]Institute for Diabetes Research and Metabolic Diseases of the Helmholtz Center Munich at the University of Tübingen, Tübingen, Germany

[2]German Center for Diabetes Research (DZD e.V.), Tübingen, Germany

[3]Department of Internal Medicine IV, University of Tübingen, Tübingen, Germany

[4]Institute of Neuroscience and Medicine – 4, Forschungszentrum Jülich GmbH, Jülich, Germany

[5]Department of Neurology, Faculty of Medicine, RWTH Aachen University, Aachen, Germany

[6]Section on Experimental Radiology, Department of Diagnostic and Interventional Radiology, University of Tübingen, Tübingen, Germany

[7]Institute of Neuroscience and Medicine – 11, Forschungszentrum Jülich GmbH, Jülich, Germany

[8]JARA – BRAIN – Translational Medicine, RWTH Aachen University, Aachen, Germany

[9]Monash Biomedical Imaging, School of Psychological Sciences, Monash University, Melbourne, VIC, Australia

[10]Department of High-Field Magnetic Resonance, Max Planck Institute for Biological Cybernetics, Tübingen, Germany

[11]Department of Biomedical Magnetic Resonance, University of Tübingen, Tübingen, Germany

[12]Institute for Clinical Chemistry and Pathobiochemistry, University Hospital Tübingen, Tübingen, Germany

[13]Institute for Diabetes and Obesity, Helmholtz Diabetes Center at Helmholtz Zentrum München, German Research Center for Environmental Health (GmbH), Neuherberg, Germany

[14]Department of Pharmacy and Biochemistry, Institute of Pharmaceutical Sciences, Eberhard Karls Universität Tübingen, Tübingen, Germany

Correspondence
Stephanie Kullmann, University of Tübingen/IDM, Otfried Müller Strasse 47, 72076 Tübingen, Germany.
Email: stephanie.kullmann@med.uni-tuebingen.de

Funding information
German Federal Ministry of Education and Research; German Center for Diabetes Research, Grant/Award Number: DZD e.V. 01GI0925; Helmholtz Alliance ICEMED-Imaging and Curing Environmental Metabolic Diseases

Abstract

There is growing evidence that obesity is associated with inflammation in the brain, which could contribute to the pathogenesis of obesity. In humans, it is challenging to detect brain inflammation in vivo. Recently, quantitative magnetic resonance imaging (qMRI) has emerged as a tool for characterising pathophysiological processes in the brain with reliable and reproducible measures. Proton density imaging provides quantitative assessment of the brain water content, which is affected in different pathologies, including inflammation. We enrolled 115 normal weight, overweight and obese men and women (body mass index [BMI] range 20.1-39.7 kg m^{-2}, age range 20-75 years, 60% men) to acquire cerebral water content mapping in vivo using MRI at 3 Tesla. We investigated potential associations between brain water content with anthropometric measures of obesity, body fat distribution and whole-body metabolism. No global changes in water content were associated with obesity. However, higher water content values in the cerebellum, limbic lobe and sub-lobular region were detected in participants with higher BMI, independent of age. More specifically,

the dorsal striatum, hypothalamus, thalamus, fornix, anterior limb of the internal capsule and posterior thalamic radiation showed the strongest relationship with BMI, independent of age. In a subgroup with available measurements (n = 50), we identified visceral adipose tissue to be the strongest tested link between higher water content values and obesity. Individuals with metabolic syndrome had the highest water content values in the hypothalamus and the fornix. There is accumulating evidence that inflammation of the hypothalamus contributed to obesity-associated insulin resistance in that area. Whether brain inflammation is a cause or consequence of obesity in humans still needs to be investigated using a longitudinal study design. Using qMRI, we were able to detect marked water content changes in young and older obese adults, which is most likely the result of chronic low-grade inflammation.

1 | INTRODUCTION

From 1975 onwards, obesity has tripled worldwide to 650 million,[1] increasing the risk of metabolic syndrome, type 2 diabetes (T2D), coronary heart disease and certain forms of cancer.[2,3] Despite tremendous efforts, an effective cure and the prevention of obesity and T2D have remained elusive. This is partly the result of a the multitude of factors that substantially contribute to the pathophysiology of obesity and T2D, including impaired insulin secretion, insulin resistance, inflammation and disproportionate body fat distribution.[4] Particularly central adiposity, a prominent trait of metabolically unhealthy obesity [4] and metabolic syndrome, is a significant source of inflammation.[5] Recent accumulating evidence shows that chronic low-grade inflammation prompts inflammatory processes in the brain, which involves non-neuronal populations such as astrocytes and microglia.[6,7] Moreover, rodent models clearly show that dietary excess can trigger brain inflammation, causing weight gain.[7,8] In humans, less is known about whether obesity is related to inflammation in the brain because it is challenging to detect subclinical brain inflammation in vivo. Thaler et al[8] were the first to describe hypothalamic gliosis in individuals with obesity using T_2-weighted magnetic resonance imaging (MRI). Subsequently, as a result of technological advances, quantitative MRI has emerged as a tool for characterising pathophysiological processes in the whole brain in vivo with reliable and reproducible measures.[9,10] The initial evidence points to water content alteration contributing to the alterations found in individuals with obesity.[11] Proton density imaging provides a quantitative assessment of the brain water content as a marker of inflammatory processes. The higher water content (ie, increased uptake of fluid can result in local swelling) may compress the distinct local microenvironments, which may finally result in dysfunctional states, accompanying various processes that damage cells.[10,12-15] In the present study, we investigated potential associations between measures of obesity and brain water content using proton density imaging to investigate potential inflammation of the entire brain. We hypothesise that individuals with obesity, especially those with visceral adiposity

and metabolic syndrome, will show increased brain water content particularly in the hypothalamus. Based on our cross-sectional design, we cannot differentiate between diet-induced or chronic inflammation.

2 | MATERIALS AND METHODS

2.1 | Participants

The study sample consisted of 115 normal weight, overweight and obese adult participants (body mass index [BMI] range 20.1-39.7 kg m$^-$^{2}, 69 men). The local ethics committee approved the protocol and informed written consent was obtained from all participants, who were recruited using broadcast emails at the University of Tübingen or through local newspaper advertisement. Participants underwent a thorough medical examination and did not suffer from psychiatric or neurological diseases. To rule out T2D, participants underwent a 75-g oral glucose tolerance test. Peripheral insulin sensitivity,[16] blood pressure and lipid profiles were additionally assessed. Metabolic syndrome was diagnosed in accordance with the International Diabetes Federation criteria.[17] It is defined by central obesity (waist circumference > 94 cm for men, > 80 cm for women) plus any two of the following risk factors: raised triglycerides, reduced high-density lipoprotein cholesterol, raised blood pressure and raised fasting glucose. Participant characteristics are summarised in Table 1 and the Supporting information (Table S1).

2.2 | Data acquisition

Studies were conducted after an overnight fast of at least 10 hours. Whole-brain MRI was obtained by using a 3 Tesla scanner (PRISMA; Siemens, Munich, Germany) with a 20-channel head coil for signal reception and the body coil for excitation. Quantitative cerebral free water (FW) content measurements were estimated based on MR-visible-proton density (PD) with an acquisition time

TABLE 1 Descriptive statistics

	Mean	SE	Minimum	Maximum
Age (years)				
Women	51.76	2.168	24	74
Men	43.43	1.605	20	75
All	46.77	0.6292	20	75
Body mass index (kg m^{-2})				
Women	27.83	0.4921	20.86	35.56
Men	26.34	0.3922	20.10	39.68
All	26.94	0.0543	20.10	39.68
HbA1c (%)				
Women	5.50	0.0477	4.70	6.40
Men	5.40	0.0361	4.40	6.40
All	5.44	1.569	4.40	6.40
Fasting glucose (mg dL^{-1})				
Women	96.63	1.073	81.00	124.0
Men	94.31	0.9014	79.00	123.0
All	95.24	1.314	79.00	124.0
oGTT-derived insulin sensitivity index				
Women	13.05	1.001	2.58	50.34
Men	13.61	0.8083	2.07	34.51
All	13.35	1.881	2.07	50.34
Waist circumference (cm)				
Women	90.06	1.597	68.00	117.0
Men	94.74	1.236	72.00	129.0
All	92.63	0.0079	68.00	129.0
Waist to hip ratio				
Women	0.865	0.0074	0.720	0.9700
Men	0.946	0.00674	0.800	1.055
All	0.909	11.448	0.720	1.055
Triglyceride (mg dL^{-1})				
Women	111.93	10.062	39	490
Men	117.02	7.534	48	367
All	114.66	5.843	39	490
Cholesterol (mg dL^{-1})				
Women	211.20	6.568	140	312
Men	198.27	4.470	103	366
All	204.27	2.220	103	366
HDL-cholesterol (mg dL^{-1})				
Women	64.51	2.067	39	100
Men	53.08	1.614	28	97
All	58.38	4.325	28	100
LDL-cholesterol (mg dL^{-1})				
Women	126.20	5.775	69	179
Men	128.42	3.673	64	302
All	127.39	43.151	64	302
Fasting free fatty acids (µmol l^{-1})				
Women	612.64	22.244	99	1650

(Continues)

TABLE 1 (Continued)

	Mean	SE	Minimum	Maximum
Men	464.50	24.366	147	865
All	533.23	2.273	99	1650
Systolic blood pressure (mm Hg)				
Women	131.91	2.148	105	162
Men	138.93	1.593	110	187
All	135.76	1.922	105	187
Diastolic blood pressure (mm Hg)				
Women	85.78	1.533	56	111
Men	85.39	1.202	64	115
All	85.57	1.685	56	115
Total adipose tissue (L)				
Women	38.33	2.151	23.60	50.90
Men	29.43	1.572	11.05	60.49
All	32.99	0.322	11.05	60.49
Visceral adipose tissue (L)				
Women	4.02	0.4581	1.69	7.46
Men	4.57	0.3003	1.31	11.07
All	4.34765	0.7424	1.31	11.07
Subcutaneous adipose tissue lower extremities				
Women	14.59550	0.7033	7.00	20.51
Men	10.92667	0.5719	4.74	20.71
All	12.39420	0.5719	4.74	20.71

Abbreviations: HDL, high-density lipoprotein; LDL, low-density lipoprotein; OGTT, oral glucose tolerance test.

of 14 minutes.[10,15] For this purpose, the water content mapping protocol was implemented using the Siemens multi-slice, multi-echo radio frequency (RF)-spoiled gradient recalled echo sequence (GRE). This method was previously validated in multiple cohorts (ranging from healthy controls to patients) using 1.5-T and 3-T MRI.[15,18]

Two proton-density-weighted (PD-w) GRE images, with inter-leaved concatenations (32 slices each), were acquired with an ac-celeration factor of 2 and 24 auto-calibration lines, TR = 1800 ms, TE = 5.8 ms, FA = 40° and bandwidth = 210 Hz per pixel. This led to 64 gap-free transverse slices of 2-mm slice thickness and 1-mm in-plane resolution measured in 6 minutes.

To quantify tissue water content, the PD-w images need to be corrected for (i) the RF field inhomogeneities; (ii) the T_2^*-contrast; and (iii) the residual T_1-contrast.

Correction 1 refers to the transmit (B_1^+) and the receive (B_1^-) pro-file. Estimation of the B_1^+ field was performed via a multiple flip angle technique.[19,20] This technique requires four echo-planar images with different FAs (30°, 60°, 90° and 120°) with a TR of 20 seconds ac-quired in approximately 1.3 minutes. The B_1^- profile is estimated by acquiring two low-resolution GRE scans (TR = 500ms, TE = 5.8 ms, BW per pixel = 210 Hz and FA = 40°, acquisition time = 30 seconds each) where the body coil was used in place of the receive head array coil for signal reception in the second acquisition.[9,10]

The correction for the T_2^* contrast was achieved by measuring the T_2^* relaxation time map using a separate RF-spoiled multi-echo 3D-GRE MR acquisition scan, with parameters of TR = 35 ms, FA = 12°, BW per pixel = 510 Hz, TE1 = 2.3 ms, ΔTE = 2.3 ms and eight echoes, acquired in 3.4 minutes (2-mm slice-thickness, 1-mm in-plane resolution). Assuming an exponential decay of the 3D-GRE, this dataset allows an estimation of the T_2^* decay constant and correction of the signal decay present in the PD-weighted scan.

Correction (c) required quantification of T_1 relaxation time. This was performed using the two-point technique.[21,22] This requires an extra T_1-weighted GRE scan, which was acquired with TR = 500 ms, TE = 5.8 ms, FA = 90° and BW per pixel = 210 Hz. Sixty-four transverse slices were acquired in two concatenations in 1.7 minutes.

For all sequences, the same orientation and field of view were used. The details about the parameters and the processing steps are provided in Abbas et al.[15] The free water content was estimated using in-house MATLAB (Mathworks, Natick, MA, USA) algorithms.

Additionally, to identify obesity-associated difference in cerebral blood flow arterial spin labelling was used, as described previously.[23] Accordingly, pulsed arterial spin labelling images were obtained with a PICORE-Q2TIPS (proximal inversion with control for off-resonance effects—quantitative imaging of perfusion by using a single subtraction) sequence using a frequency offset corrected inversion pulse and echo-planar imaging readout for acquisition.[24]

2.3 | Data processing

2.3.1 | Estimation of the relaxation parameters and total free water content

Following the T_1, T_2^* and transmit/receiver profiles corrections, the PD-weighted scan cannot yet be treated as a quantitative water content map because it requires further correction for receiver bias profile maps.[9,10] This is achieved by exploiting the linear relationship between corrected PD-weighted contrast and T_1 relaxation time in certain brain regions (60 ms > T_2^* > 50 ms).[9,15]

Finally, the calibration of the bias-free water content map was performed using a robust and reliable approach.[9,15] It uses the regions within cerebrospinal fluid based on T_1, T_2^* thresholds and its stability in terms of transmit profile. The calibration factor was then computed via the weighted average across the stable regions.

All quantitative free water content and T_1 maps were normalised using SPM12.

2.3.2 | Cerebral blood flow quantification

Image preprocessing was performed using ASLTBX [24] with SPM12 (Wellcome Trust Centre for Neuroimaging, London, UK).[23] We used the general kinetic model for absolute perfusion quantification, as reported previously.[25] Perfusion images were generated by calculating the control-tag differences by using surround subtraction. For accurate CBF quantification (mL × 100g^{-1} × min^{-1}), we used an M0 map to quantify the perfusion on each voxel.

2.3.3 | Body fat assessment by whole-body MRI

On a separate day, a subgroup (n = 50) underwent whole-body MRI to assess body fat distribution of the participants. These MRI examinations were performed on a 1.5-T whole-body imager (Magnetom Sonata; Siemens Healthineers, Erlangen, Germany). A whole-body imaging protocol was used to record a set of 90-120 T_1-weighted axial slices. This approach enabled quantification of body volume, total adipose tissue (TAT) and total mass of specific fat depots such as subcutaneous (s.c. adipose tissue of the lower extremities (SCAT$_{LE}$) ranging from feet to femoral heads, and visceral adipose tissue (VAT) via an automated segmentation algorithm, applying fuzzy clustering and orthonormal snakes.[26,27]

2.4 | Statistical analysis

Region-of-interests (ROIs) were selected from the Wake Forest Pickatlas[28] to extract quantitative FW values of 11 brain lobes (temporal, sub-lobar, pons, parietal, occipital, midbrain, medulla, limbic, frontal-temporal space, frontal lobe and parts of the cerebellum within the field of view during data acquisition) and seven subcortical regions: bilateral thalamus, dorsal and ventral striatum, amygdala, hippocampus, and the lateral and medial hypothalamus. ROIs of white matter tracts were selected from the JHU-DTI based white matter atlases[29,30] (JHU-ICBM labels 1 mm) to extract quantitative FW values of 48 white matter tracts. Additionally, FW values of total grey (GM) and white matter (WM) were extracted for the calculation of ratios (FW values displayed in the Supporting information, Table S2). In total, 66 ratios were created to compare the mean quantitative FW values within the ROIs with total grey matter or white matter tissue as a control region. Correlation analysis was performed between the 66 ratios and BMI, presence of the metabolic syndrome and MR-based body fat distribution (visceral adipose tissue and non-VAT tissue). Non-parametric bivariate correlations and partial correlations with Spearman rho was used for analysis in SPSS, version 25 (IBM Corp., Armonk, NY, USA). Correlations were considered significant if they survived a threshold of $P \leq 0.0007$ ($P = 0.05$ corrected for number of ROIs; n = 66). To estimate the effect size of the relationship between BMI and the change in quantitative FW, the linear coefficient (slope) was calculated. In a similar vein, baseline quantitative cerebral blood flow was extracted for each region of interest and correlated with measures of obesity.

3 | RESULTS

3.1 | Higher water content with increasing BMI in grey and white matter regions

In our sample of 115 adults, no significant associations of global water content of the brain with measures of obesity were observed.

Instead, we observed regional specific associations (Figure 1). Of the different brain lobes, the cerebellum and sub-lobular region (which includes striatal regions and hypothalamus) showed higher cerebral free water content values with increasing BMI independent of age and sex (cerebellum: $r_{sp} = 0.434$, $P < 0.0007$; sub-lobular: $r_{sp} = 0.420$, $P < 0.0007$). Further region of interests, namely the lateral hypothalamus ($r_{sp} = 0.439$, $P < 0.0007$) (Figure 2), dorsal striatum ($r_{sp} = 0.394$, $P < 0.0007$) and thalamus ($r_{sp} = 0.441$, $P < 0.0007$), showed a significant positive relationship with BMI independent of age and sex (Table 2). The BMI-correlated increase in FW amounted to 0.006 (p.u.) per BMI point (calculated slope). Furthermore, FW values of white matter tracts showed a significant positive association with BMI independent of age and sex, most significantly the fornix ($r_{sp} = 0.419$, $P < 0.0007$) (Figure 2), left anterior limb of the internal capsule ($r_{sp} = 0.334$, $P < 0.0007$) and right posterior thalamic radiation ($r_{sp} = 0.346$, $P < 0.0007$) (Table 2).

3.2 | Individuals with metabolic syndrome display increased hypothalamic and thalamic water content values

We divided the sample of 115 individuals into three groups: individuals with metabolic syndrome (13 women and 18 men), individuals with central obesity who did not fulfill diagnostic criteria for metabolic syndrome (23 women and 12 men) and healthy non-obese individuals (10 women, 39 men). We identified the highest water content values in the hypothalamus ($r_{sp} = 0.344$, $P < 0.0007$), thalamus ($r_{sp} = 0.327$, $P < 0.0007$) and fornix ($r_{sp} = 0.357$, $P < 0.0007$) in individuals with metabolic syndrome adjusted for age and sex (Figure 3).

3.3 | Individuals with higher visceral fat content or lower s.c. adipose tissue mass display increased free water content

In a subgroup with available measurements (n = 50), we investigated the association between water content values and MR-based fat distribution $SCAT_{LE}$ and VAT independent of the amount of TAT. The most significant associations were found for the lateral hypothalamus water content with VAT ($r = 0.440$, $P = 0.001$) and $SCAT_{LE}$ ($r = -.532$, $P < 0.0007$) independent of the amount of TAT and with the right posterior thalamic radiation (for VAT: $r = 0.479$, for $SCAT_{LE}$: $r = -.518$, $P < 0.0007$), left tapetum (for VAT: $r = 0.556$, for $SCAT_{LE}$: $r = -.402$, $P < 0.0007$) and right tapetum (for VAT: $r = 0.566$, $P < 0.0007$; for $SCAT_{LE}$: $r = -0.452$, $P = 0.001$). Hence, individuals with more visceral and less s.c. fat in the lower extremities showed the highest water content (for details, see the Supporting information, Table S3). After adjusting for sex and age, correlations did not remain significant ($P > 0.05$, uncorrected).

3.4 | No significant association between baseline cerebral blood flow and obesity

Based on the arterial spin labelling measure, we identified no significant differences between cerebral blood flow of the different brain regions and BMI, presence of the metabolic syndrome or MR-based body fat distribution ($P > 0.05$) (data not shown). The mean $\pm$ SD cerebral blood flow value of the total grey matter was 33.12 ± 0.79 mL $\times$ 100 g^{-1} $\times$ min^{-1}.

FIGURE 1 Brain structures affected by increased free water content in obesity overlayed on a mean quantitative proton density map (A, anterior limb of internal capsule; D, dorsal striatum, including caudate and putamen; F, fornix; H, lateral hypothalamus; MCP, middle cerebellar peduncle; P, posterior thalamic radiation; Th, thalamus)
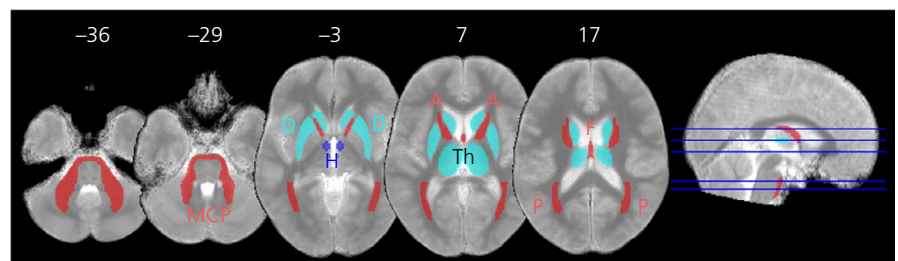

FIGURE 2 Free water content associates with obesity. Correlation plots show positive relationship between body mass index (BMI) and free water values in the lateral hypothalamus/total grey matter signal ratio (on left) and the fornix/total white matter signal ratio (on right). Line represents the fit line. Correlation values are based on Spearman rho; plots are not adjusted for age and sex
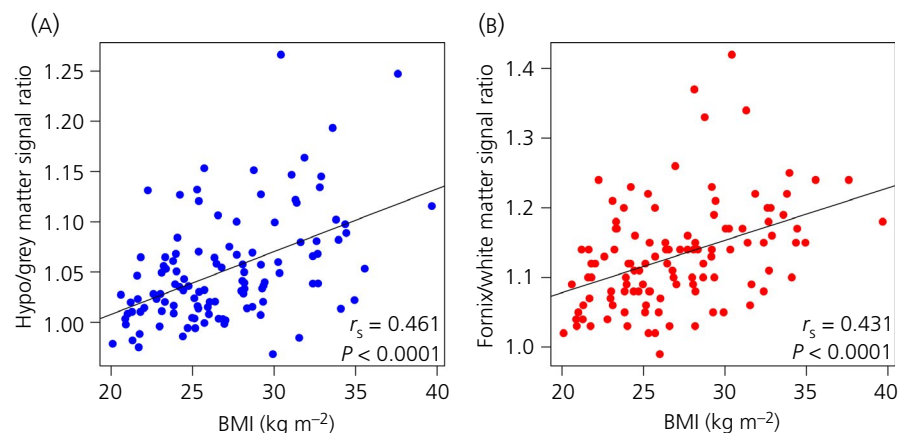
(A) Hypo/grey matter signal ratio vs BMI (kg m^{-2}): $r_s = 0.461$, $P < 0.0001$

(B) Fornix/white matter signal ratio vs BMI (kg m^{-2}): $r_s = 0.431$, $P < 0.0001$

TABLE 2 Relationship between FW values and body mass index (BMI)

Anatomical regions	BMI	Age	Sex	BMI$_{adj for age and sex}$
Region-of-interests/total grey matter ratio				
Amygdala				
Correlation coefficient	0.013	−0.150	0.137	0.06
P value (two-sided)	0.891	0.110	0.143	0.524
Dorsal striatum				
Correlation coefficient	0.422	0.446	−0.052	0.394
P value (two-sided)	< 0.0007	< 0.0007	.578	< 0.0007[§]
Hippocampus				
Correlation coefficient	0.282	0.232	0.055	0.269
P value (two-sided)	0.002	0.013	0.563	0.004
Lateral hypothalamus				
Correlation coefficient	0.461	0.558	−0.033	0.439
P value (two-sided)	< 0.0007	< 0.0007	0.731	< 0.0007[§]
Medial hypothalamus				
Correlation coefficient	0.291	0.634	0.026	0.262
P value (two-sided)	0.002	< 0.0007	0.781	0.005
Thalamus				
Correlation coefficient	0.460	0.659	−0.236	0.441
P value (two-sided)	< 0.0007	< 0.0007	.011	< 0.0007[§]
Ventral striatum				
Correlation coefficient	0.189	0.042	0.005	0.188
P value (two-sided)	0.044	0.658	0.955	0.046
Talairach Daemon lobes/total grey matter ratio				
Cerebellum (anterior part)				
Correlation coefficient	0.463	0.281	−0.091	0.434
P value (two-sided)	< 0.0007	0.002	0.331	< 0.0007[§]
Frontal temporal space				
Correlation coefficient	−0.159	0.082	0.194	−0.152
P value (two-sided)	0.090	0.384	0.038	0.109
Frontal				
Correlation coefficient	−0.054	0.306	−0.121	−0.131
P value (two-sided)	0.570	0.001	0.196	0.166
Limbic				
Correlation coefficient	0.355	0.185	−0.181	0.316
P value (two-sided)	< 0.0007	0.048	0.053	0.001
Midbrain				
Correlation coefficient	0.329	0.508	−0.196	0.263
P value (two-sided)	< 0.0007	< 0.0007	0.036	0.005
Occipital				
Correlation coefficient	−0.154	−0.466	0.166	−0.063
P value (two-sided)	0.100	< 0.0007	0.076	0.507
Parietal				
Correlation coefficient	0.014	−0.155	−0.198	0.010
P value (two-sided)	0.884	0.098	0.034	0.917

TABLE 2 (Continued)

Anatomical regions	BMI	Age	Sex	BMI$_{adj for}$ age and sex
Pons				
Correlation coefficient	0.271	0.175	0.021	0.258
P value (two-sided)	0.003	0.061	0.825	0.006
Sub lobular				
Correlation coefficient	0.446	0.575	−0.132	0.420
P value (two-sided)	< 0.0007	< 0.0007	0.159	< **0.0007**[§]
Temporal				
Correlation coefficient	−0.045	−0.229	−0.109	−0.026
P value (two-sided)	0.630	0.014	0.246	0.781
JHU-ICBM labels/total white matter ratio				
Middle cerebellar peduncle				
Correlation coefficient	0.250	−0.128	0.203	0.318
P value (two-sided)	0.007	0.173	0.030	0.001
Pontine crossing tract				
Correlation coefficient	0.199	0.078	0.065	0.204
P value (two-sided)	0.033	0.410	0.489	0.030
Genu of corpus callosum				
Correlation coefficient	0.188	0.473	0.021	0.136
P value (two-sided)	0.044	< 0.0007	0.821	0.151
Body of corpus callosum				
Correlation coefficient	0.271	0.542	−0.060	0.214
P value (two-sided)	0.003	< 0.0007	0.521	0.023
Splenium of corpus callosum				
Correlation coefficient	0.217	0.176	0.051	0.206
P value (two-sided)	0.020	0.060	0.590	0.028
Fornix				
Correlation coefficient	0.431	0.375	0.029	0.419
P value (two-sided)	< 0.0007	< 0.0007	0.759	< **0.0007**[§]
Corticospinal tract, right				
Correlation coefficient	0.109	−0.081	0.056	0.135
P value (two-sided)	0.247	0.388	0.551	0.155
Corticospinal tract, left				
Correlation coefficient	0.025	0.008	0.030	0.029
P value (two-sided)	0.789	0.928	0.751	0.759
Medial lemniscus, right				
Correlation coefficient	0.246	0.133	0.009	0.235
P value (two-sided)	0.008	0.158	0.923	0.012
Medial lemniscus, left				
Correlation coefficient	0.200	0.138	−0.048	0.177
P value (two-sided)	0.032	0.141	0.610	0.060
Inferior cerebellar peduncle, right				
Correlation coefficient	0.347	0.182	−0.118	0.316
P value (two-sided)	< 0.0007	0.052	0.211	0.001

(Continues)

TABLE 2 (Continued)

Anatomical regions	BMI	Age	Sex	BMI_{adj for age and sex}
Inferior cerebellar peduncle, left				
Correlation coefficient	0.176	0.268	−0.139	0.120
P value (two-sided)	0.060	0.004	0.138	0.205
Superior cerebellar peduncle, right				
Correlation coefficient	0.152	0.270	0.112	0.136
P value (two-sided)	0.105	0.004	0.234	0.151
Superior cerebellar peduncle, left				
Correlation coefficient	0.053	0.281	0.082	0.022
P value (two-sided)	0.571	0.002	0.382	0.816
Cerebral peduncle, right				
Correlation coefficient	0.197	0.275	−0.044	0.156
P value (two-sided)	0.035	0.003	0.642	0.098
Cerebral peduncle, left				
Correlation coefficient	0.111	0.256	−0.163	0.049
P value (two-sided)	0.238	0.006	0.082	0.608
Anterior limb of internal capsule, right				
Correlation coefficient	0.305	0.356	−0.024	0.270
P value (two-sided)	< 0.0007	< 0.0007	0.161	0.002
Anterior limb of internal capsule, left				
Correlation coefficient	0.345	0.309	0.067	0.334
P value (two-sided)	< 0.0007	0.001	0.478	< 0.0007[§]
Posterior limb of internal capsule, right				
Correlation coefficient	0.337	0.577	−0.132	0.283
P value (two-sided)	< 0.0007	< 0.0007	0.161	0.002
Posterior limb of internal capsule, left				
Correlation coefficient	0.333	0.475	−0.283	0.257
P value (two-sided)	< 0.0007	< 0.0007	0.002	0.006
Retrolenticular part of internal capsule, right				
Correlation coefficient	0.298	0.384	0.159	0.301
P value (two-sided)	0.001	< 0.0007	0.090	0.001
Retrolenticular part of internal capsule, left				
Correlation coefficient	0.019	0.076	−0.172	−0.020
P value (two-sided)	0.842	0.420	0.067	0.833
Anterior corona radiata, right				
Correlation coefficient	0.036	0.369	−0.216	−0.063
P value (two-sided)	0.706	< 0.0007	0.020	0.507
Anterior corona radiata, left				
Correlation coefficient	0.263	0.444	−0.057	0.211
P value (two-sided)	0.005	< 0.0007	0.547	0.025
Superior corona radiata, right				
Correlation coefficient	0.133	0.580	−0.141	0.023
P value (two-sided)	0.156	< 0.0007	0.132	0.806

TABLE 2 (Continued)

Anatomical regions	BMI	Age	Sex	BMI_adj for age and sex
Superior corona radiata, left				
Correlation coefficient	0.137	0.582	−0.228	0.011
P value (two-sided)	0.146	< 0.0007	0.014	0.910
Posterior corona radiata, right				
Correlation coefficient	0.180	0.495	0.206	0.167
P value (two-sided)	0.054	< 0.0007	0.027	0.077
Posterior corona radiata, left				
Correlation coefficient	−0.037	0.333	0.001	−0.100
P value (two-sided)	0.691	< 0.0007	0.991	0.293
Posterior thalamic radiation, right				
Correlation coefficient	0.310	0.565	0.207	0.340
P value (two-sided)	0.001	< 0.0007	0.026	< **0.0007**[§]
Posterior thalamic radiation, left				
Correlation coefficient	0.100	0.580	0.054	0.019
P value (two-sided)	0.288	< 0.0007	0.566	0.844
Sagittal stratum, right				
Correlation coefficient	0.213	0.363	0.218	0.218
P value (two-sided)	0.022	< 0.0007	0.019	0.020
Sagittal stratum, left				
Correlation coefficient	0.066	0.308	0.017	0.021
P value (two-sided)	0.481	0.001	0.856	0.826
External capsule, right				
Correlation coefficient	−0.050	−0.179	0.200	0.010
P value (two-sided)	0.598	0.056	0.032	0.920
External capsule, left				
Correlation coefficient	−0.003	−0.231	0.114	0.054
P value (two-sided)	0.974	0.013	0.226	0.568
Cingulum (cingulate gyrus), right				
Correlation coefficient	0.030	0.048	−0.044	0.016
P value (two-sided)	0.749	0.610	0.638	0.864
Cingulum (cingulate gyrus), left				
Correlation coefficient	−0.027	−0.027	−0.004	−0.024
P value (two-sided)	0.775	0.771	0.964	0.802
Cingulum (hippocampus), right				
Correlation coefficient	0.256	−0.105	0.210	0.321
P value (two-sided)	0.006	0.264	0.025	0.001
Cingulum (hippocampus), left				
Correlation coefficient	0.005	−0.153	−0.050	0.024
P value (two-sided)	0.955	0.102	0.598	0.803
Fornix (cres)/Stria terminalis, right				
Correlation coefficient	0.210	0.288	0.176	0.211
P value (two-sided)	0.024	0.002	0.060	0.025

TABLE 2 (Continued)

Anatomical regions	BMI	Age	Sex	BMI$_{adj for}$ age and sex
Fornix (cres)/Stria terminalis, left				
Correlation coefficient	0.138	0.157	0.044	0.124
P value (two-sided)	0.143	0.094	0.638	0.189
Superior longitudinal fasciculus, right				
Correlation coefficient	0.214	0.100	−0.064	0.195
P value (two-sided)	0.021	0.287	0.499	0.038
Superior longitudinal fasciculus, left				
Correlation coefficient	−0.025	0.171	−0.162	−0.081
P value (two-sided)	0.789	0.067	0.084	0.392
Superior fronto-occipital fasciculus, right				
Correlation coefficient	0.177	0.650	−0.091	0.080
P value (two-sided)	0.058	< 0.0007	0.331	0.401
Superior fronto-occipital fasciculus, left				
Correlation coefficient	0.220	0.531	−0.019	0.161
P value (two-sided)	0.018	< 0.0007	0.838	0.089
Uncinate fasciculus, right				
Correlation coefficient	−0.262	−0.413	0.249	−0.182
P value (two-sided)	0.005	< 0.0007	0.007	0.054
Uncinate fasciculus, left				
Correlation coefficient	−0.112	−0.307	0.198	−0.036
P value (two-sided)	0.232	0.001	0.034	0.703
Tapetum, right				
Correlation coefficient	0.169	0.429	0.228	0.164
P value (two-sided)	0.070	< 0.0007	0.014	0.083
Tapetum, left				
Correlation coefficient	0.075	0.381	0.163	0.044
P value (two-sided)	0.423	< 0.0007	0.082	0.641

Note: Table shows non-parametric correlations using Spearman rho; §partial correlations significant after correcting for number of regions investigated (critical P value of 0.0007).

4 | DISCUSSION

Obesity and its associated comorbidities, such as insulin resistance and dyslipidaemia, are known to individually associate with changes in brain structure and function,[31,32] although the underlying cause of the observed effects remains inconclusive. In the present study, we used whole-brain proton density imaging to quantify brain water content in 115 normal weight, overweight and obese individuals. We found obesity-associated measures to positively correlate with brain water content, mainly in the subcortical and cerebellar regions and the white matter tracts connecting these regions. Individuals with obesity, particularly those with visceral obesity and altered lipid profiles, showed an enhanced water content in spatially discrete brain regions and white matter tracts, including the cerebellum, hypothalamus, striatum, thalamus, fornix, anterior limb of internal capsule and posterior thalamic radiation. In accordance with our hypothesis, the hypothalamus and white matter tracts surrounding the hypothalamus displayed the most prominent alterations in water content. However, our results additionally show that brain inflammation is not restricted to the hypothalamic area and also affects the surrounding brain regions. This coincides with structural MRI studies showing that individuals with obesity and metabolic syndrome exemplify grey matter atrophy primarily in the cerebellum and subcortical regions[31] and show reduced white matter integrity in fibres connecting these regions.[11,32,33]

Although the underlying cause still remains elusive, genetic factors, as well as cellular and cerebrovascular mechanisms, contribute to this deteriorating brain health seen in obesity.[32] In this context, inflammation has gained particular notoriety as a potential cellular mechanism leading to neuronal atrophy and compromised white matter integrity.[34] However, inflammation in the brain does not replicate the usual process seen in the periphery with the recruitment of peripheral immune cells. This is largely a result of the presence of
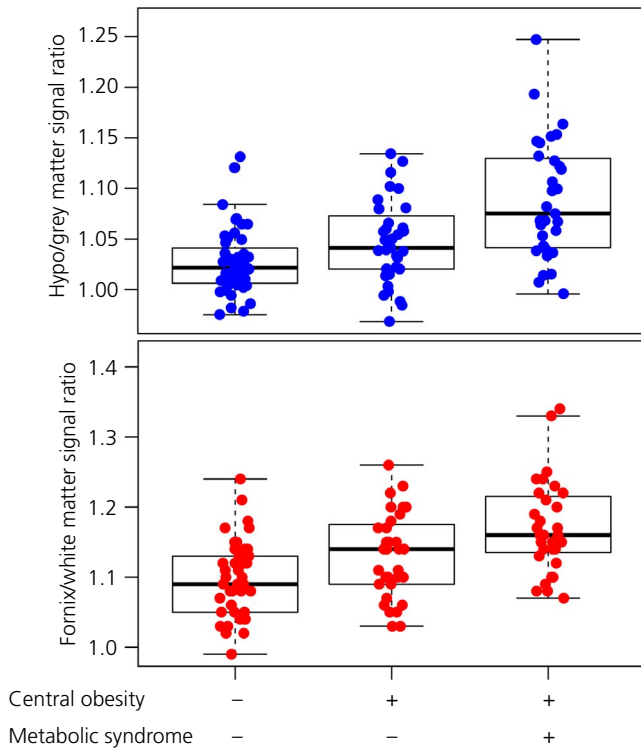
| Central obesity | − | + | + |
| Metabolic syndrome | − | − | + |

FIGURE 3 Box plots showing hypothalamic and fornix water content for healthy non-obese individuals without central obesity or metabolic syndrome (n = 49), for individuals with central obesity (n = 35; based on IDF criteria using waist circumference) and for individuals with metabolic syndrome (n = 31). Individuals with metabolic syndrome have central obesity plus two further metabolic risk factors, such as raised triglycerides, reduced high-density lipoprotein cholesterol, raised blood pressure or raised fasting plasma glucose. These individuals have significant higher free water values than healthy non-obese persons, as well as individuals with central obesity without metabolic syndrome

the blood-brain barrier limiting the entry of immune cells to the brain in the healthy state.[35] Instead, inflammation in the brain involves activation of glial cells (microglia and astrocytes), which are able to produce inflammatory mediators.[6,7,36] Microglial cells are considered resident immune cells of the brain, whereas astrocytes are the most numerous cells in the brain performing many functions, including the modulation of the blood-brain barrier. Animal studies using diet-induced obesity models show increased blood-brain barrier permeability and glial activation in the hypothalamus, hippocampus, amygdala, brainstem, cerebellum and cortex with increased inflammatory markers.[35] Moreover, neurones are also directly affected by hyperphagia with decreased neurogenesis[37] and less dendritic complexity.[38] These models in rodents confirm that diet-induced hypothalamic inflammation is causally related to hyperphagia and weight gain, making it a model of obesity pathogenesis.[39] In addition to diet-induced hyperphagia, chronic low-grade inflammation, caused by obesity and unhealthy fat distribution, can promote inflammatory processes in numerous tissues including the brain.[35]

To detect brain inflammation in humans, we take advantage of the fact that the response of glia cells results in increased water uptake

with local swelling. This can damage the cell by compressing distinct microenvironments.[18] Quantitative MRI techniques are sensitive with respect to detecting local changes in brain water content,[18,40] located in multiple tissues, including neurones, axons, myelin sheaths, extracellular space, blood vessels and glial cells. Most abundantly, water diffusion, as assessed by diffusion tensor imaging (DTI) measurements, has been used to evaluate obesity-associated changes in white matter structures. These studies reveal a negative impact of obesity on white matter microstructure regardless of age, particularly in tracts of the limbic system and those connecting temporal and frontal lobes.[33] However, it is difficult to disentangle the contribution of changes in water and myelin content in DTI metrics. To explore specific brain tissue properties, quantitative MRI techniques are implemented to specifically investigate the contribution of water content to the MRI signal.[11] Within the white matter, the initial evidence points to an increase in water rather than a decrease myelin in young adults with obesity.[11] However, very little is known about changes in water content within the grey matter. Thaler et al[8] were the first to investigate potential hypothalamus inflammation, by means of a measure often implemented in standard diagnostics (ie, T_2-relaxation time over a limited field of view). Obese volunteers revealed a hyperintensity (longer T_2-relaxation time) in the hypothalamus compared to a control region. The hypothalamic signal significantly correlated positively with BMI,[8] the magnitude of peripheral insulin resistance[41,42] and systemic low-grade inflammation.[43] Importantly, MRI postmortem scans and histological staining confirmed that the signal detected by in vivo MRI is a valid surrogate measure for hypothalamic inflammation.[41] The findings of the present study are in agreement with these previous findings, revealing an increased hypothalamic free water content (higher proton density values compared to the control region) in individuals with obesity independent of age and sex. Moreover, our results show that water content is elevated in subcortical regions and white matter tracts connecting homeostatic and limbic system. Whether brain inflammation is reversible is currently not known. The initial evidence suggests that some aspects of neuroinflammation can be rescued in both humans and rodents.[35,42] However, it is not known whether this is the result of direct central effects or is caused by decreased peripheral inflammation. Moreover, Kreutzer et al[43] did not identify this beneficial effect because the hypothalamic signal remained increased after bariatric surgery. It is currently not known which factors contribute to improved gliosis in response to an intervention. It is postulated that metabolic health prior to the intervention plays a critical role, particularly components of the metabolically unhealthy phenotype such as insulin resistance and abdominal obesity.[42] In the present study, especially metabolically unhealthy individuals show the greatest increase in brain water content, particularly in the hypothalamus and surrounding white matter tracts. Insulin signalling in the brain is blunted in individuals with obesity in similar regions as identified in the present study. Particularly, individuals with central obesity show brain insulin resistance in subcortical regions,[23,44,45] with negative consequences on peripheral metabolism.[46-49] Whether brain inflammation contributes to insulin resistance in the brain or vice versa currently remains unknown.

Other proposed mechanisms to explain structural and function changes in obesity include cerebrovascular mechanisms. Core features of the metabolic syndrome, such as insulin resistance and dyslipidaemia, can lead to endothelial dysfunction, along with vascular reactivity and cerebral blood flow.[32] In our present sample, however, we did not observe any changes in regional or global cerebral blood flow in individuals with obesity. This emphasises that it is most likely inflammation, rather than cerebrovascular mechanisms, that led to our current findings.

A limitation of the method used in our cohort was the presence of motion artefacts in MR images, especially in obese patients, as a result of breathing. However, the MR images were visually inspected and the datasets with no visible motion artifacts were selected for the analysis. Because of the cross-sectional design of the study, no cause-effect relationship can be established between obesity and brain inflammation, such that we cannot distinguish between brain inflammation induced by dietary excess or chronic low-grade inflammation; a sequel of obesity and excess adipose tissue. Further longitudinal studies are required to investigate whether this inflammatory process can be manipulated acutely through diet, weight loss and pharmaceutical interventions, with potential benefits for further health.

In conclusion, we postulate that chronic low-grade inflammation, as observed in obesity, metabolic syndrome and diabetes, also affects the brain, which may facilitate further weight gain and brain insulin resistance.[50] In 115 volunteers, we observed an increase in local water content in individuals with obesity. Remarkably, this local increase is specifically found in subcortical regions; further supporting the idea that inflammation in the brain may be a cause of altered brain function and structure.

ACKNOWLEDGEMENTS

CONFLICT OF INTERESTS

The authors declare that they have no conflicts of interest.

PEER REVIEW

The peer review history for this article is available at https://publons.com/publon/10.1111/jne.12907.

DATA AVAILABILITY

The data that support the findings of this study are available on reasonable request from the corresponding author. The data are not publicly available as a result of privacy or ethical restrictions.

ORCID

Stephanie Kullmann (ID) https://orcid.org/0000-0001-9951-923X

Hubert Preissl (ID) https://orcid.org/0000-0002-8859-4661

REFERENCES

1. World Health Organization. *Obesity and Overweight*. Geneva, Switzerland: World Health Organization. 2018. http://www.who.int/mediacentre/factsheets/fs311/en/. Accessed December 9, 2019.
2. Flegal KM, Graubard BI, Williamson DF, Gail MH. Excess deaths associated with underweight, overweight, and obesity. *JAMA*. 2005;293:1861-1867.
3. Flegal KM, Carroll MD, Ogden CL, Curtin LR. Prevalence and trends in obesity among US adults, 1999–2008. *JAMA*. 2010;303:235-241.
4. Stefan N, Fritsche A, Schick F, Haring HU. Phenotypes of prediabetes and stratification of cardiometabolic risk. *Lancet Diabetes Endocrinol*. 2016;4:789-798.
5. Alexopoulos N, Katritsis D, Raggi P. Visceral adipose tissue as a source of inflammation and promoter of atherosclerosis. *Atherosclerosis*. 2014;233:104-112.
6. Garcia-Caceres C, Balland E, Prevot V, et al. Role of astrocytes, microglia, and tanycytes in brain control of systemic metabolism. *Nat Neurosci*. 2019;22:7-14.
7. Seong J, Kang JY, Sun JS, Kim KW. Hypothalamic inflammation and obesity: a mechanistic review. *Arch Pharm Res*. 2019;42:383-392.
8. Thaler JP, Yi CX, Schur EA, et al. Obesity is associated with hypothalamic injury in rodents and humans. *J Clin Invest*. 2011;122:153-162.
9. Abbas Z, Gras V, Mollenhoff K, Keil F, Oros-Peusquens AM, Shah NJ. Analysis of proton-density bias corrections based on T1 measurement for robust quantification of water content in the brain at 3 Tesla. *Magn Reson Med*. 2014;72:1735-1745.
10. Neeb H, Ermer V, Stocker T, Shah NJ. Fast quantitative mapping of absolute water content with full brain coverage. *NeuroImage*. 2008;42:1094-1109.
11. Kullmann S, Callaghan MF, Heni M, et al. Specific white matter tissue microstructure changes associated with obesity. *NeuroImage*. 2016;125:36-44.
12. Lerski RA, Straughan K, Orr JS. Calibration of proton density measurements in nuclear magnetic resonance imaging. *Phys Med Biol*. 1984;29:271-276.
13. Tofts P. *Quantitative MRI of the Brain: Measuring Changes Caused by Disease*. Chichester, GB: John Wiley & Sons; 2004.
14. Mezer A, Yeatman JD, Stikov N, et al. Quantifying the local tissue volume and composition in individual brains with magnetic resonance imaging. *Nat Med*. 2013;19:1667-1672.
15. Abbas Z, Gras V, Mollenhoff K, Oros-Peusquens AM, Shah NJ. Quantitative water content mapping at clinically relevant field strengths: a comparative study at 1.5 T and 3 T. *NeuroImage*. 2015;106:404-413.
16. Matsuda M, DeFronzo RA. Insulin sensitivity indices obtained from oral glucose tolerance testing: comparison with the euglycemic insulin clamp. *Diabetes Care*. 1999;22:1462-1470.
17. Alberti KGMM, Zimmet P, Shaw J; Group IDFETFC. The metabolic syndrome–a new worldwide definition. *Lancet*. 2005;366:1059-1062.
18. Reetz K, Abbas Z, Costa AS, et al. Increased cerebral water content in hemodialysis patients. *PLoS One*. 2015;10:e0122188.
19. Gras V, Abbas Z, Shah NJ. Spoiled FLASH MRI with slice selective excitation: signal equation with a correction term. *Concept Magn Reson A*. 2013;42:89-100.
20. Weber H, Paul D, Elverfeldt DV, Hennig J, Zaitsev M. Extended multi-flip-angle B-1 mapping: a 3D mapping method for inhomogeneous B-1 fields. *Concept Magn Reson B*. 2010;37B:203-214.
21. Parker GJM, Barker GJ, Tofts PS. Accurate multislice gradient echo T(1) measurement in the presence of non-ideal RF pulse shape and RF field nonuniformity. *Magnet Reson Med*. 2001;45:838-845.
22. Deoni SCL, Rutt BK, Peters TM. Rapid combined T-1 and T-2 mapping using gradient recalled acquisition in the steady state. *Magnet Reson Med*. 2003;49:515-526.

23. Kullmann S, Heni M, Veit R, et al. Selective insulin resistance in homeostatic and cognitive control brain areas in overweight and obese adults. *Diabetes Care*. 2015;38:1044-1050.

24. Wang Y, Saykin AJ, Pfeuffer J, et al. Regional reproducibility of pulsed arterial spin labeling perfusion imaging at 3T. *NeuroImage*. 2011;54:1188-1195.

25. Frank S, Linder K, Kullmann S, et al. Fat intake modulates cerebral blood flow in homeostatic and gustatory brain areas in humans. *Am J Clin Nutr*. 2012;95:1342-1349.

26. Machann J, Thamer C, Schnoedt B, et al. Standardized assessment of whole body adipose tissue topography by MRI. *J Magn Reson Imaging*. 2005;21:455-462.

27. Wurslin C, Machann J, Rempp H, Claussen C, Yang B, Schick F. Topography mapping of whole body adipose tissue using A fully automated and standardized procedure. *J Magn Reson Imaging*. 2010;31:430-439.

28. Maldjian JA, Laurienti PJ, Kraft RA, Burdette JH. An automated method for neuroanatomic and cytoarchitectonic atlas-based interrogation of fMRI data sets. *NeuroImage*. 2003;19:1233-1239.

29. Hua K, Zhang J, Wakana S, et al. Tract probability maps in stereotaxic spaces: analyses of white matter anatomy and tract-specific quantification. *NeuroImage*. 2008;39:336-347.

30. Wakana S, Caprihan A, Panzenboeck MM, et al. Reproducibility of quantitative tractography methods applied to cerebral white matter. *NeuroImage*. 2007;36:630-644.

31. Kotkowski E, Price LR, Franklin C, et al. A neural signature of metabolic syndrome. *Hum Brain Mapp*. 2019;40:3575-3588.

32. Alfaro FJ, Gavrieli A, Saade-Lemus P, Lioutas VA, Upadhyay J, Novak V. White matter microstructure and cognitive decline in metabolic syndrome: a review of diffusion tensor imaging. *Metabolism*. 2018;78:52-68.

33. Kullmann S, Schweizer F, Veit R, Fritsche A, Preissl H. Compromised white matter integrity in obesity. *Obes Rev*. 2015;16:273-281.

34. Yates KF, Sweat V, Yau PL, Turchiano MM, Convit A. Impact of metabolic syndrome on cognition and brain: a selected review of the literature. *Arterioscler Thromb Vasc Biol*. 2012;32:2060-2067.

35. Guillemot-Legris O, Muccioli GG. Obesity-induced neuroinflammation: beyond the hypothalamus. *Trends Neurosci*. 2017;40:237-253.

36. Jha MK, Lee WH, Suk K. Functional polarization of neuroglia: implications in neuroinflammation and neurological disorders. *Biochem Pharmacol*. 2016;103:1-16.

37. Murata Y, Narisawa Y, Shimono R, et al. A high fat diet-induced decrease in hippocampal newly-born neurons of male mice is exacerbated by mild psychological stress using a Communication Box. *J Affect Disord*. 2017;209:209-216.

38. Jeon BT, Jeong EA, Shin HJ, et al. Resveratrol attenuates obesity-associated peripheral and central inflammation and improves memory deficit in mice fed a high-fat diet. *Diabetes*. 2012;61:1444-1454.

39. Valdearcos M, Douglass JD, Robblee MM, et al. Microglial inflammatory signaling orchestrates the hypothalamic immune response to dietary excess and mediates obesity susceptibility. *Cell Metab*. 2018;27:1356.

40. Shah NJ, Neeb H, Kircheis G, Engels P, Haussinger D, Zilles K. Quantitative cerebral water content mapping in hepatic encephalopathy. *NeuroImage*. 2008;41:706-717.

41. Schur EA, Melhorn SJ, Oh SK, et al. Radiologic evidence that hypothalamic gliosis is associated with obesity and insulin resistance in humans. *Obesity (Silver Spring)*. 2015;23:2142-2148.

42. van de Sande-Lee S, Melhorn SJ, Rachid B, et al. Radiologic evidence that hypothalamic gliosis is improved after bariatric surgery in obese women with type 2 diabetes. *Int J Obes (Lond)*. 2020;44(1):178–185.

43. Kreutzer C, Peters S, Schulte DM, et al. Hypothalamic inflammation in human obesity is mediated by environmental and genetic factors. *Diabetes*. 2017;66:2407-2415.

44. Kullmann S, Heni M, Hallschmid M, Fritsche A, Preissl H, Haring HU. Brain insulin resistance at the crossroads of metabolic and cognitive disorders in humans. *Physiol Rev*. 2016;96:1169-1209.

45. Heni M, Kullmann S, Preissl H, Fritsche A, Haring HU. Impaired insulin action in the human brain: causes and metabolic consequences. *Nat Rev Endocrinol*. 2015;11:701-711.

46. Heni M, Wagner R, Willmann C, et al. Brain insulin action stimulates pancreatic insulin secretion: results from hyperglycaemic clamps. *Diabetologia*. 2018;61:S72.

47. Heni M, Wagner R, Kullmann S, et al. Hypothalamic and striatal insulin action suppresses endogenous glucose production and may stimulate glucose uptake during hyperinsulinemia in lean but not in overweight men. *Diabetes*. 2017;66:1797-1806.

48. Kullmann S, Fritsche A, Wagner R, et al. Hypothalamic insulin responsiveness is associated with pancreatic insulin secretion in humans. *Physiol Behav*. 2017;176:134-138.

49. Heni M, Wagner R, Kullmann S, et al. Central insulin administration improves whole-body insulin sensitivity via hypothalamus and parasympathetic outputs in men. *Diabetes*. 2014;63:4083-4088.

50. Jais A, Bruning JC. Hypothalamic inflammation in obesity and metabolic disease. *J Clin Invest*. 2017;127:24-32.

SUPPORTING INFORMATION

Additional supporting information may be found online in the Supporting Information section.